Composite Materials and Engineering, *Vol. 2, No. 1 (2020) 13-24*
DOI: https://doi.org/10.12989/cme.2020.2.1.013

Buckling of non-sway Euler composite frame with semi-rigid connection

Mostafa G. Ghadimi*

Department of Civil Engineering, Sarab Branch, Islamic Azad University, Sarab, Iran

(Received May 1, 2019, Revised September 20, 2019, Accepted October 5, 2019)

Abstract. The stability functions are calculated to obtain critical elastic buckling loads of asymmetric and axisymmetric one-span non-sway bending frames made up of laminated thin beams and columns with through-thickness mechanical properties variation subjected to axial compression. The shear and axial deformations are neglected. It is assumed that the members are perfect and axial compression is applied to neutral axis without eccentricity. The relative rotations of beams with respect to columns are occurred due to semi-rigid connections at joints of the bending frame. The perfect connection of two different rectangular thin plates with the same width and dissimilar elasticity modulus and thickness produces intact laminated members with similar curvature at junction of the plates in the buckled member. The mechanical and geometrical properties of laminated members in axial direction are invariant, as result the stiffness coefficient, modified stiffness coefficient, reduced stiffness coefficient and carry over factor are independent from thickness, length and layers' mechanical properties variations, but critical buckling loads of heterogeneous frames are dependent on these parameters. The results show that the dimensionless critical load of heterogeneous frame is same as the dimensionless critical load of homogeneous frame.

Keywords: buckling; non-sway bending frame; axisymmetric and asymmetric shape modes; semi-rigid connection; composite member; stability function

1. Introduction

The initial bending may change the lateral buckling load. In the previous studies, it is shown that the elastic buckling load of symmetric portal frame is affected by the initial bending, noticeably. In the case of anti-symmetric frames the changes are not so seriously like the symmetric frames (Chilver 1956). Lack of adequate information or conservative methods for the efficient design of steel structures against out-of-plane failure is an important issue. The method of design by buckling analysis can improve this situation. The design by buckling analysis can use member nominal design strengths in terms of the section moment capacities or compression capacities and the maximum moments at elastic buckling (Trahair 2009). In general, a two-step approach is applied to perform buckling analysis of steel frame. Firstly, a linear-elastic analysis is done to calculate the internal forces and moments; and secondly, an initial imperfection is considered to perform the buckling analysis and design for each individual element of the frame. In the steel design codes the element effective length factor K, depends on the buckling shape of that particular element within the

*Corresponding author, MSc, E-mail: mostafa.ghanizade.ghadimi@gmail.com

Copyright © 2020 Techno-Press, Ltd.
http://www.techno-press.org/?journal=cme&subpage=7 ISSN: 2671-4930 (Print), 2671-5120 (Online)

structure, and in practical cases it is obtained by means of approximations or even by mere estimation. Some researchers introduce a direct one-step method for the buckling analysis of steel frame structures by neglecting length factor via perform a non-linear analysis starting from an initial deformation state that includes the initial imperfections of the elements (Bayo and Loureiro 2001). The behavior of columns in steel building frames is inelastic at the buckling stage. After considering the overall frame inelastic stability, the true safety factor can be obtained. As a result, the individual column effective length factors, and their true slenderness ratios can be computed, and used in the design relationships. This procedure starts with a stability analysis and gradually modifies the structural properties to take account of inelasticity and eventually converges to the final buckling factor and mode shape (Farshi and Kooshesh 2009). The highest resistance against buckling in the single buckling mode columns and frames of a given volume can be obtained by solving the eigenvalue problem via finite element method in an iterative optimization process (Szyszkowski and Watson 1998). The geometric and material nonlinear analyses are used to study instability of braced frames by accounting for member initial bow, initial sway imperfection and residual stresses. The relationship between the bracing rigidity and ultimate load capacity as well as minimum bracing stiffness corresponding to the non-sway buckling mode is found. Also it is found that the horizontal load produces extras bracings' stresses, and thus makes the bracings yield prematurely and results in mode shape changing and decrease of bracing stiffness (Tong and Xing 2007). The performance of structures made of novel materials like the FGM is increased due to improving their properties. As result, the analysis of these types of structures is in focus (Heydari 2009, 2015, 2015, 2018, 2019, She *et al*. 2018, She *et al*. 2018, She *et al*. 2018, She *et al*. 2018). Many researches are conducted to investigate buckling and vibration behaviors of the structural members (Heydari 2011, 2013, 2017, Heydari *et al*. 2017, Heydari 2018a, 2018b, Heydari and Shariati 2018).

In this paper, buckling behavior of the asymmetric one story and axisymmetric two story composite bending frames with semi-rigid connections at joints made of thin members with uniform thicknesses and rectangular sections subjected to uniaxial compression without eccentricity are investigated. It is assumed that the roof of each story is confined by restraint; therefore the first mode shape is drift excluded. In addition, members are made up of two different metallic layers with the same width. The transversely heterogeneous beams and columns are produced by these layers. Because of the through-thickness variation of mechanical properties of materials the neutral axis is not coincident to the mid-axis and this imposes the more difficulties in the analytical solutions. Moreover, the bending rigidity should be calculated by considering the physical concept of neutral axis. In the case of thin members, the Euler-Bernoulli beam theory is applied and consequently the extras shear deformations and rotations are neglected due to small amount of shear stress in comparison to the normal stresses. By using these assumptions the distortion is ignored. The curvature of each point is the second derivative of deflection of that point. In the thin heterogeneous members, the perpendicular line to the neutral axis remains straight without any relative rotation with respect to the neutral axis. The above mentioned assumptions make it possible to explain equilibrium equation with only one ordinary differential equation. The axial load is imposed without eccentricity and it is perpendicular to the cross section. After deriving basic equations, the critical buckling load is calculated. The comparison between critical loads of non-sway in-homogeneous bending frame and homogeneous bending frame for similar boundary conditions and geometrical properties can be conducted by considering ratio of equivalent bending rigidity to flexural rigidity of homogeneous frame. The outcomes are presented by depicting figures and tables.

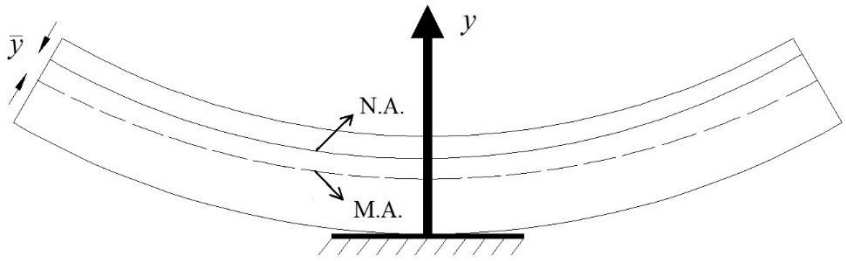

Fig. 1 The composite member subjected to pure bending

2. Governing equations

In Fig. 1, the origin of *y*, is located at bottom fiber of the laminated member. The distance between neutral axis (N.A.) and mid-axis (M.A.) is equal to $\bar{y}$. The parameter L denotes length of the heterogeneous member. The is equal to ρ. The in-homogeneous member is made up of two metallic layers with the same width b. The depth or total thickness of section is equal to H. The thickness and modulus of elasticity of layers are equal to $t1$, $t2$ and $E1$, $E2$ respectively.

The equilibrium of infinitesimal axial forces is presented in Eq. (1).

$$\mathrm{E_1}\int_0^{\mathrm{t_1}}\left(-\frac{\mathrm{y}-(\bar{\mathrm{y}}+\mathrm{H}/2)}{\rho}\right)\mathrm{dy}+\mathrm{E_2}\int_{\mathrm{t_1}}^{\mathrm{d}}\left(-\frac{\mathrm{y}-(\bar{\mathrm{y}}+\mathrm{H}/2)}{\rho}\right)\mathrm{dy}=0 \tag{1}$$

The ordinate of N.A. ($\bar{Y}=\bar{y}+H/2$) is calculated from Eq. (1) as follows

$$\bar{\mathrm{Y}}=\frac{\mathrm{E_1t_1^2}+\mathrm{E_2t_2^2}+2\mathrm{E_2t_2t_1}}{2(\mathrm{E_2t_2}+\mathrm{E_1t_1})} \tag{2}$$

The bending moment is introduced in Eq. (3).

$$\mathrm{M_z}=\int\sigma_{\mathrm{x}}\mathrm{ydA}=\mathrm{E_1}\int_0^{\mathrm{t_1}}\left(-\frac{\mathrm{y}-\bar{\mathrm{Y}}}{\rho}\right)\mathrm{ydy}+\mathrm{E_2}\int_{\mathrm{t_1}}^{\mathrm{t_1+t_2}}\left(-\frac{\mathrm{y}-\bar{\mathrm{Y}}}{\rho}\right)\mathrm{y\,dy} \tag{3}$$

After substituting Eq. (2) in Eq. (3), the radius of curvature, ρ, is calculated as follows

$$\rho=(\mathrm{E_1^2t_1^4}+4\mathrm{E_1E_2t_1^3t_2}+6\mathrm{E_1E_2t_1^2t_2^2}+4\mathrm{E_1E_2t_1t_2^3}+\mathrm{E_2^2t_2^4})/\big(12\mathrm{M_z}(\mathrm{E_2t_2}+\mathrm{E_1t_1})\big) \tag{4}$$

Bending rigidity is equal to product of curvature radius and bending moment. The bending rigidity for heterogeneous rectangular section with the width b is calculated in Eq. (5). The parameters $\bar{E}=E_2/E_1$ and $\bar{t}=t_1(H-t_1)/H^2$ are used to simplify formulae. In the case of $E_1=E_2=E$ the rigidity of homogeneous member i.e., $Eb\mathrm{H}^3/12$ will be obtained.

$$\mathrm{EI_{eq}}=\mathrm{bE_1}(\mathrm{t_1^4}+2\bar{\mathrm{E}}\bar{\mathrm{t}}(2-\bar{\mathrm{t}})\mathrm{d}^4+\bar{\mathrm{E}}^2\mathrm{t_2^4})/\big(12(\bar{\mathrm{E}}\mathrm{t_2}+\mathrm{t_1})\big) \tag{5}$$

The support reactions of pinned-clamped laminated composite beam subjected to axial compression is presented in Fig. 2.

The equilibrium ODE of the member is written in right-handed coordinate system as follows

$$\frac{\mathrm{d}^2}{\mathrm{dx}^2}\,\mathrm{y(x)}+\frac{\mathrm{P}}{\mathrm{EI_{eq}}}\mathrm{y(x)}=\left((1+\mathrm{c})\frac{\mathrm{x}}{\mathrm{L}}-1\right)\frac{\mathrm{s}\theta_{\mathrm{A}}}{\mathrm{L}} \tag{6}$$

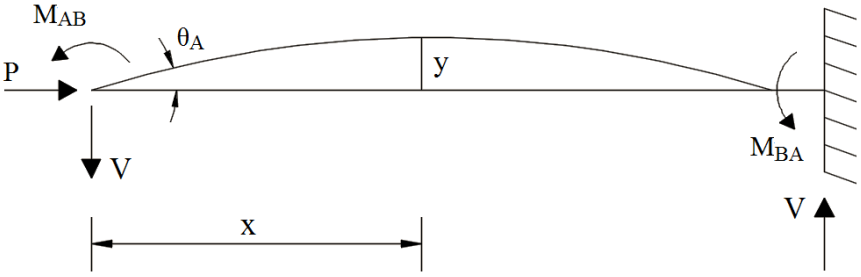

Fig. 2 The reactions of pinned-clamped buckled beam

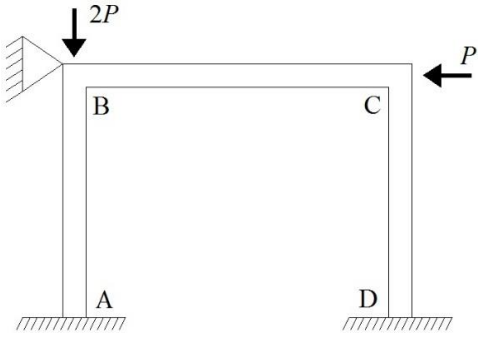

Fig. 3 Asymmetric and non-sway heterogeneous bending frame

The parameters s and c are stiffness coefficient and carry over factor, respectively. After applying boundary conditions at the ends, $y(0) = y(L) = 0$, the solution of Eq. (6) will be obtained. The ratio of buckling load of heterogeneous member to the Euler buckling load is assumed equal to n. One can write $y'(0) = \theta_A$ and $y'(L) = 0$, as result the parameters *s* and *c* can be obtained as follows

$$s = \frac{\sqrt{n}\pi\left(\sqrt{n}\pi - \tan\left(\sqrt{n}\pi\right)\right)}{\sqrt{n}\pi\tan\left(\sqrt{n}\pi\right) + 2\left(1 - \sec\left(\sqrt{n}\pi\right)\right)} \tag{7}$$

$$c = \frac{\tan\left(\sqrt{n}\pi\right) - \sqrt{n}\pi\sec\left(\sqrt{n}\pi\right)}{\sqrt{n}\pi - \tan\left(\sqrt{n}\pi\right)} \tag{8}$$

A one story asymmetric and non-sway laminated bending frame is presented in Fig. 3. The axial load of the right column is negligible with respect to the other members. The axial load of the left column is two times of the beam axial load. Fig. 4 shows the bending moment distribution at joints. Two independent equilibrium equations of bending moments at joints are written in Eq. (9). Since beam has the relative rotations with respect to the columns at joints *B* and *C*, the parameters α_B and α_C are applied in the equilibrium equations to model the semi-rigid connections. The relative rotation decreases bending stiffness of the beam at joints; therefore the reduction stiffness parameters α_B and α_C take real values between 0 and 1. For the case that joints have a rigid connection without any relative rotation, the parameters are approached to 1. For hinge joint, the parameters α_B and α_C are equal to zero.

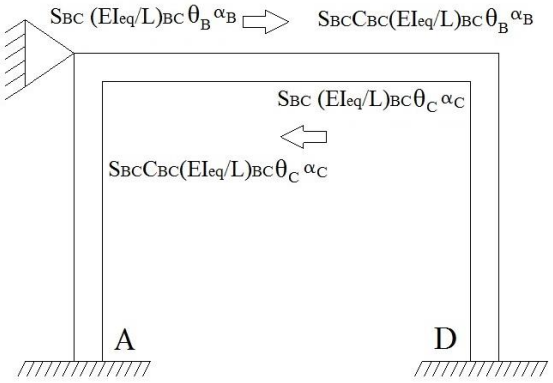

Fig. 4 Bending moment distribution in buckled frame

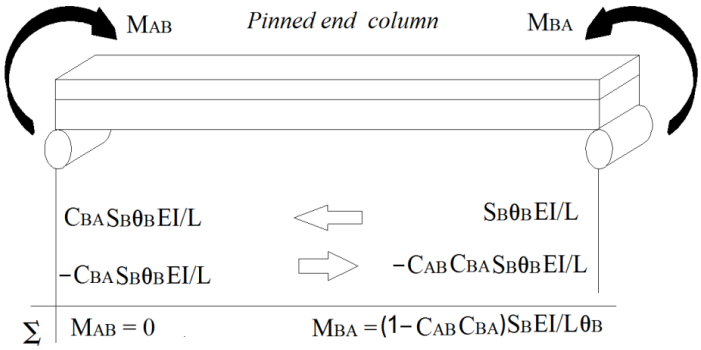

Fig. 5 The reduced stiffness factor for pinned end

$$\begin{bmatrix} s_{AB}\left(\frac{EI_{eq}}{L}\right)_{AB} + s_{BC}\alpha_B\left(\frac{EI_{eq}}{L}\right)_{BC} & s_{BC}c_{BC}\alpha_C\left(\frac{EI_{eq}}{L}\right)_{BC} \\ s_{BC}c_{BC}\alpha_B\left(\frac{EI_{eq}}{L}\right)_{BC} & 4\left(\frac{EI_{eq}}{L}\right)_{CD} + s_{BC}\alpha_C\left(\frac{EI_{eq}}{L}\right)_{BC} \end{bmatrix}\begin{bmatrix}\theta_b \\ \theta_c\end{bmatrix} = \begin{bmatrix}0 \\ 0\end{bmatrix} \tag{9}$$

The nontrivial solution implies that the determinant of the coefficient matrix in Eq. (9) must be vanished.

$$\left(s_{AB}\left(\frac{EI_{eq}}{L}\right)_{AB} + s_{BC}\alpha_B\left(\frac{EI_{eq}}{L}\right)_{BC}\right)\left(4\left(\frac{EI_{eq}}{L}\right)_{CD} + s_{BC}\alpha_C\left(\frac{EI_{eq}}{L}\right)_{BC}\right) - \left(s_{BC}c_{BC}\left(\frac{EI_{eq}}{L}\right)_{BC}\right)^2 \alpha_B\alpha_C = 0 \tag{10}$$

The relation between dimensionless critical load of beam and left column is as follows

$$\frac{n_{AB}}{n_{BC}} = 2\frac{(EI_{eq})_{BC}}{(EI_{eq})_{AB}}\left(\frac{L_{AB}}{L_{BC}}\right)^2 \tag{11}$$

In the case of column with pinned end, the reduced stiffness factor after using moment distribution is calculated in Fig. 5.

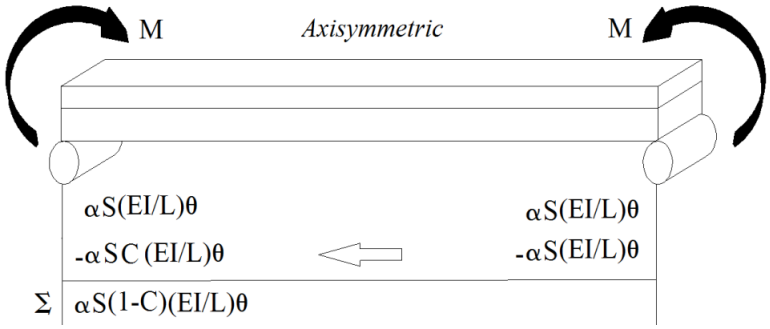

Fig. 6 The modified stiffness factor for axisymmetric beam

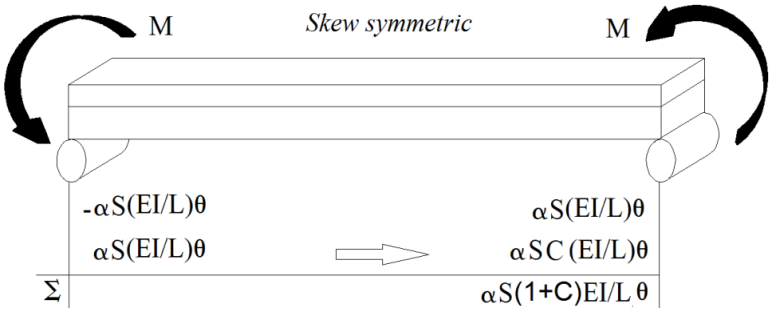

Fig. 7 The modified stiffness factor for skew symmetric beam

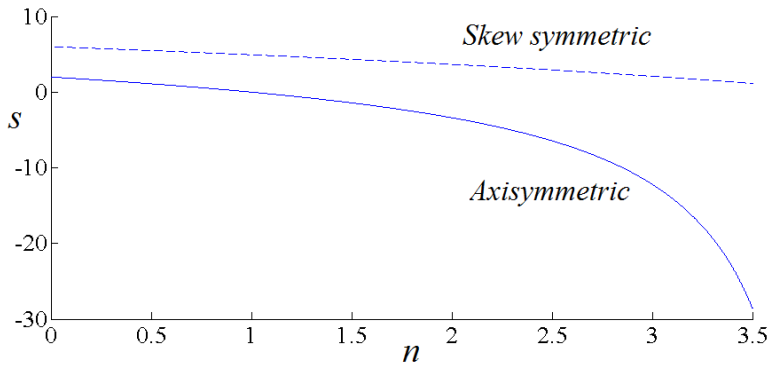

Fig. 8 The modified stiffness factors for skew symmetric and axisymmetric conditions

Also, the modified stiffness factors of the beam for axisymmetric and skew symmetric conditions are calculated in Fig. 6 and Fig. 7, respectively.

According to Fig. 8, the stiffness factor for the skew symmetric condition is more than stiffness factor for the axisymmetric condition; therefore the skew symmetric mode shape is corresponding to higher modes.

The stiffness matrix of axisymmetric two story frames illustrated in Fig. 9(a) and Fig. 9(b) with similar members by considering half of the frames are presented in Eq. (12) and Eq. (13).

$$\begin{bmatrix} s(2n) + 2\alpha + 4 & 2 \\ 2 & \alpha\tilde{s}(n) + 4 \end{bmatrix} EI_{eq}/L \tag{12}$$

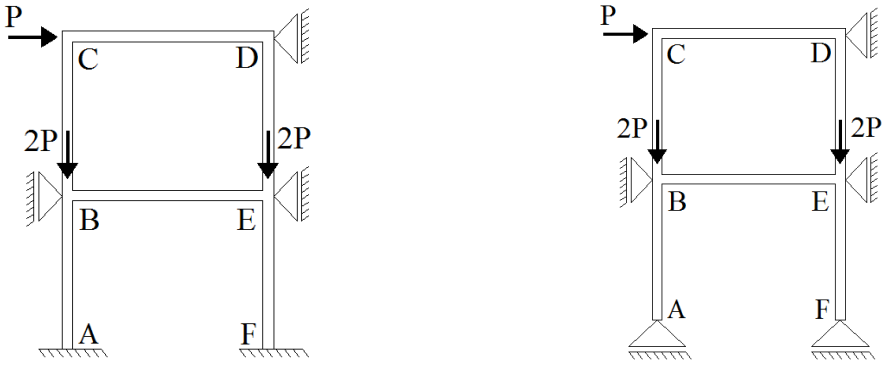

Fig. 9 Two story heterogeneous bending frame with semi-rigid connections (Load pattern I) (a): clamped (b): pinned

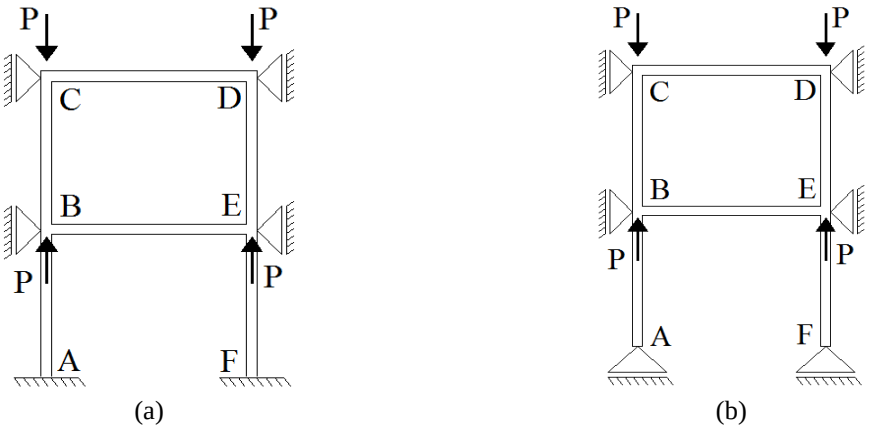

Fig. 10 Two story inhomogeneous frame with semi-rigid connections (Load pattern II) (a): clamped (b): pinned

$$\begin{bmatrix} \bar{s}(2n) + 2\alpha + 4 & 2 \\ 2 & \alpha\tilde{s}(n) + 4 \end{bmatrix} EI_{eq}/L \tag{13}$$

The parameters $\tilde{s}$ and $\bar{s}$ are modified stiffness and reduced stiffness coefficients. The characteristic equations in Eqs. (14) and (15) are calculated by using nontrivial solution ($n_{AB} = 2n_{CD} = 2n$).

$$(s(2n) + 2\alpha + 4)(\alpha\tilde{s}(n) + 4) - 4 = 0 \tag{14}$$

$$(\bar{s}(2n) + 2\alpha + 4)(\alpha\tilde{s}(n) + 4) - 4 = 0 \tag{15}$$

The characteristic equations of axisymmetric bending frames in Fig. 10(a) and 10(b) are calculated in Eq. (16) and Eq. (17), respectively.

$$(2\alpha + 8)\big(2\alpha + s(n)\big) - s(n)c(n) \times s(n)c(n) = 0 \tag{16}$$

$$(2\alpha + 7)\big(2\alpha + s(n)\big) - s(n)c(n) \times s(n)c(n) = 0 \tag{17}$$

3. Results and discussions

For the numerical analysis the numerical values of dimensions and elasticity moduli in terms of m and GPa are presented in Table 1.

Table 1 Numerical values of geometry and mechanical properties

AB					*BC*					*CD*				
E_1	E_2	t_1	t_2	L	E_1	E_2	t_1	t_2	L	E_1	E_2	t_1	t_2	L
120	150	0.02	0.03	3.5	300	400	0.02	0.04	2.5	100	120	0.03	0.02	3.5

Table 2 shows the effect of semi-rigid connections on critical load of asymmetric non-sway bending frame for the case that the same connections are used at both joints *B* and *C* (i.e., $\alpha_B = \alpha_C$).

Table 2 critical load of asymmetric frame for various amounts of α ($\alpha_B = \alpha_C = \alpha$)

α	0	0.1	0.2	0.3	0.4	0.5	0.6	0.7	0.8	0.9	1
P (MN)	1.150	1.445	1.611	1.721	1.800	1.859	1.904	1.940	1.970	1.994	2.015

Table 3 shows the effect of semi-rigid connections on critical load of asymmetric non-sway bending frame for $\alpha_B = 0.5\alpha_C$.

Table 3 critical load of asymmetric frame for various amounts of α_c ($\alpha_B = 0.5\alpha_C$)

α_c	0	0.1	0.2	0.3	0.4	0.5	0.6	0.7	0.8	0.9	1
P (MN)	1.150	1.316	1.432	1.522	1.595	1.656	1.707	1.750	1.787	1.820	1.848

Table 4 shows the effect of semi-rigid connections on critical load of asymmetric non-sway bending frame for $\alpha_B = 2\alpha_C$.

Table 4 critical load of asymmetric frame for various amounts of α_B ($\alpha_B = 2\alpha_C$)

α_B	0	0.1	0.2	0.3	0.4	0.5	0.6	0.7	0.8	0.9	1
P (MN)	1.150	1.457	1.629	1.7395	1.817	1.873	1.917	1.952	1.980	2.003	2.023

Fig. 11 illustrates the critical load variations against degree of rigidity for ($\alpha_C = 0.2\alpha_B$), schematically.

The dimensionless critical load of axisymmetric frames presented in Fig. 9(a) and Fig. 9(b) is depicted in Fig. 12. The clamped and simply supported conditions are presented by (C-C) and (S-S), respectively. The similar diagrams for load pattern II are illustrated in Fig. 13.

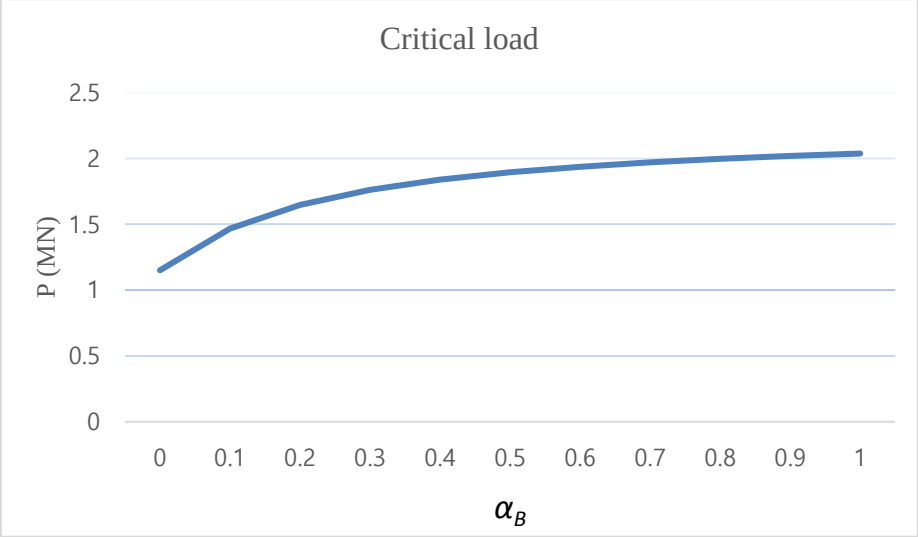

Fig. 11 Critical load of asymmetric one story non-sway frame with semi-rigid connections

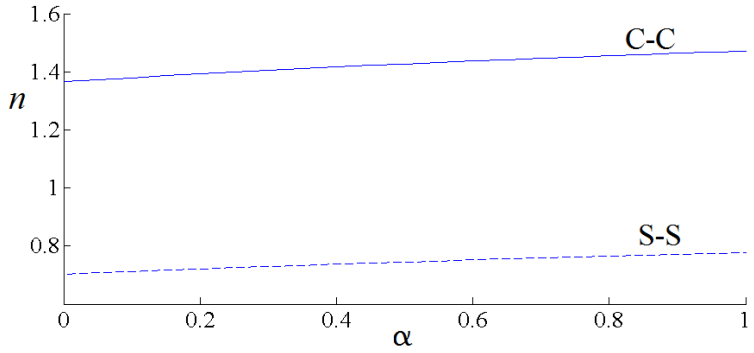

Fig. 12 Dimensionless critical load of two story frames (Load Pattern I)

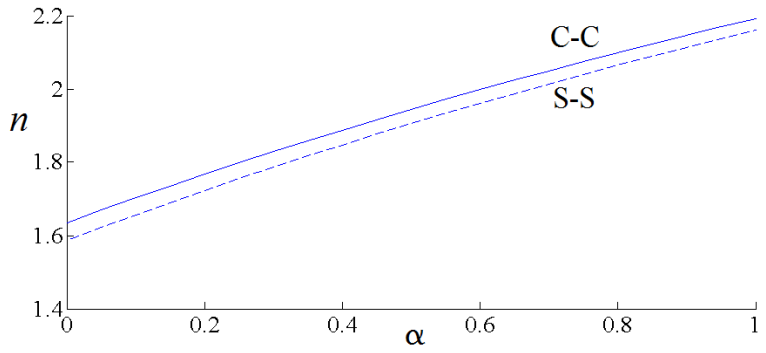

Fig. 13 Dimensionless critical load of two story frames (Load Pattern II)

The ratio of the critical load of laminated frame to critical load of homogeneous frame with similar boundary conditions and geometrical properties is equal to ratio of the equivalent bending

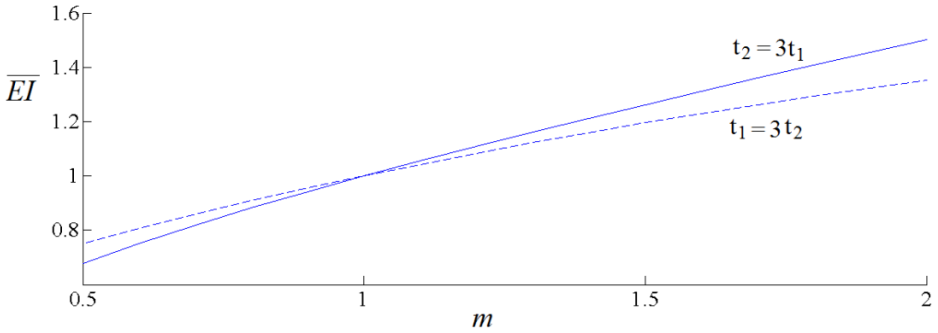

Fig. 14 The critical load of laminated frame to critical load of homogeneous frame ratio

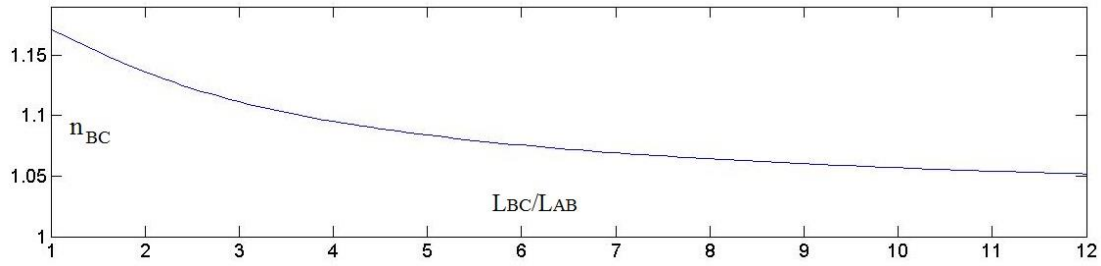

Fig. 15 The effect of beam to column ratio on critical load of asymmetric bending frame

rigidity to flexural rigidity of homogeneous frame. Fig. 14 illustrates the effect of the inhomogeneity on critical load ($E_2 = mE_1$). The parameter $\overline{EI}$ is equal to the ratio of EI_{eq} to $E_1 bH^3/12$. Fig. 15 presents the effect of the beam length to column length on the critical load of the asymmetric frame in Fig. 3 for $L_{AB} = 1$. The dimensionless critical load of the frame is expressed in terms of the dimensionless critical load of the beam, which is decreased by increasing beam length to column length ratio.

4. Conclusions

In current study, the buckling behavior of one story asymmetric and two story axisymmetric laminated bending frames with semi-rigid connections at joints by neglecting drift at ceiling levels is investigated. The analytical formulas for neutral axis location, equivalent flexural rigidity, stiffness coefficient, reduced and modified stiffness coefficients and carry over factor of laminated members are computed. The members are assumed to be through-thickness heterogeneous. In contrast to the above-mentioned coefficients, critical load is depended on through-thickness inhomogeneity. The critical load is increased by increasing of the degree of rigidity.

References

Abbas, H. (2009), "Elasto-plastic analysis of thick walled tanks subjected to internal pressure", *Int. J. Adv. Des. Manuf. Technol.*, **3**(1), 11-18.

Abbas, H. (2011), "Buckling of functionally graded beams with rectangular and annular sections subjected to axial compression", *Int. J. Adv. Des. Manuf. Technol.*, **5**(1), 25-31.
Abbas, H. (2013), "Analytical solutions for buckling of functionally graded circular plates under uniform radial compression by using Bessel function", *Int. J. Adv. Des. Manuf. Technol.*, **6**(4), 41-47.
Abbas, H. (2015), "Spreading of plastic zones in functionally graded spherical tanks subjected to internal pressure and temperature gradient combinations", *Iran. J. Mech. Eng. Tran. ISME*, **16(**2), 5-25.
Abbas, H. (2015), "Thermo-elasto-plastic analysis of functionally graded spherical reservoirs subjected to temperature gradient", *10th International Congress on Civil Engineering*, Tabriz, Iran.
Abbas, H. (2017), "A new scheme for buckling analysis of bidirectional functionally graded euler beam having arbitrary thickness variation rested on hetenyi elastic foundation", *Modares Mech. Eng.*, **17**(1), 47-55.
Abbas, H. (2018), "Elastoplastic analysis of thick-walled vessels with isotropic strain hardening behavior using nonlinear compatibility relation", *7th International Conference on Civil Engineering, Architecture and Urban Economy Development*, Shiraz, Iran.
Abbas, H. (2018), "Exact vibration and buckling analyses of arbitrary gradation of nano-higher order rectangular beam", *Steel Compos. Struct.*, **28**(5), 589-606.
Abbas, H. (2018), "Size-dependent damped vibration and buckling analyses of bidirectional functionally graded solid circular nano-plate with arbitrary thickness variation", *Struct. Eng. Mech.*, **68**(2), 171-182.
Abbas, H. (2019), "Elasto-plastic analysis of cylindrical vessel with arbitrary material gradation subjected to thermo-mechanical loading via DTM", *Arab. J. Sci. Eng.*, **44(**10), 8875-8891.
Bayo, E. and Loureiro, A. (2001), "An efficient and direct method for buckling analysis of steel frame structures", *J. Constr. Steel Res.*, **57**(12), 1321-1336.
Chilver, A.H. (1956), "Buckling of a simple portal frame", *J. Mech. Phys. Solid.*, **5**(1), 18-25.
Farshi, B. and Kooshesh, F. (2009), "Buckling analysis of structural steel frames with inelastic effects according to codes", *J. Constr. Steel Res.*, **65(**10), 2078-2085.
Heydari, A. and Shariati, M. (2018), "Buckling analysis of tapered BDFGM nano-beam under variable axial compression resting on elastic medium", *Struct. Eng. Mech.*, **66**(6), 737-748.
Heydari, A., Jalali, A. and Nemati, A. (2016), "Buckling analysis of circular functionally graded plate under uniform radial compression including shear deformation with linear and quadratic thickness variation on the Pasternak elastic foundation", *Appl. Math. Model.*, **41**, 494-507.
She, G.L., Ren, Y.R., Xiao, W.S. and Liu, H. (2018), "Study on thermal buckling and post-buckling behaviors of FGM tubes resting on elastic foundations", *Struct. Eng. Mech.*, **66**(6), 729-736.
She, G.L., Ren, Y.R., Yuan, F.G. and Xiao, W.S. (2018), "On vibrations of porous nanotubes", *Int. J. Eng. Sci.*, **125**, 23-35.
She, G.L., Yuan, F.G. and Ren, Y.R. (2018), "On wave propagation of porous nanotubes", *Int. J. Eng. Sci.*, **130**, 62-74.
She, G.L., Yuan, F.G., Ren, Y.R., Liu, H.B. and Xiao, W.S. (2018), "Nonlinear bending and vibration analysis of functionally graded porous tubes via a nonlocal strain gradient theory", *Compos. Struct.*, **203**, 614-623.
Szyszkowski, W. and Watson, L.G. (1988), "Optimization of the buckling load of columns and frames", *Eng. Struct.*, **10**(4), 249-256.
Tong, G.S. and Xing, G.R. (2007), "Determination of buckling mode for braced elastic-plastic frames", *Eng. Struct.*, **29**(10), 2487-2496.
Trahair, N.S. (2009), "Buckling analysis design of steel frames", *J. Constr. Steel Res.*, **65**(7), 1459-1463.

CC

Symbols

$M.A.$ Mid-axis

$N.A.$	Neutral axis
$\bar{y}$	Distance between $M.A.$ and $N.A.$
L	Member length
ρ	Curvature radius
w	Width
H	Total thickness
t_1	First layer thickness
t_2	Second layer thickness
E_1	Elasticity modulus of first layer
E_2	Elasticity modulus of second layer
$\bar{Y}$	Ordinate of $N.A.$
P	Axial compression load
V	Shear load in buckled member
M_z	Bending moment in buckled member
$\bar{E}$	Dimensionless elasticity modulus (E_2/E_1)
$\bar{t}$	Dimensionless thickness $(t_1(H-t_1)/H^2)$
$\overline{EI}$	Buckling load ratio of heterogeneous frame to homogeneous frame
EI_{eq}	Equivalent bending rigidity
y	Buckling deflection
θ	Rotation at pinned end
s	Stiffness coefficient
c	Carry over factor
α	Reduction stiffness parameter
$\tilde{s}$	Modified stiffness coefficient
$\bar{s}$	Reduced stiffness coefficient
n	Dimensionless buckling load